Journal of
Nanoscience and Nanotechnology
Vol. 12, 2548–2556, 2012

Formation of Ag Nanoframes with Facilitation of Dithiols

Fong-Yu Cheng[1,2], Kuo-Wei Hu[2], and Chen-Sheng Yeh[2,*]

[1] Institute of Oral Medicine, National Cheng Kung University, Tainan 701, Taiwan
[2] Department of Chemistry and Center for Micro/Nano Science and Technology, National Cheng Kung University, Tainan 701, Taiwan

Two-dimensional Ag nanoprisms readily formed Ag triangular nanoframes upon electron beam irradiation. Following meso-2, 3-dimercaptosuccinicacid (DMSA) ripening behavior, continuous electron beam exposure transformed a solid nanoplate into a core/void/shell morphology, which then evolved into a hollow nanoframe structure. TEM was used to observe the ripening and etching processes of Ag nanoprisms as a function of DMSA concentration and electron irradiation time. X-ray diffraction (XRD) and FT-IR analysis were conducted to characterize the Ag nanoprism structure and surface before and after treatment with DMSA. X-ray photoelectron spectroscopy (XPS) was used to determine surface chemical compositions and indicated DMSA was adsorbed on the Ag nanoprisms in the form of Ag^{+}–S^{-}. Raman measurements provided evidence of a disulfide group on Ag nanoprisms. Similar organosulfur structures such as mercaptosuccinic acid and 2-mercaptoacetic acid were also studied with results suggesting that the two S-H groups of dithiol DMSA played the crucial role in nanoframe fabrication. Using the same strategy with DMSA, the nano-architecture can be extended to 2D nanodiscs yielding nanorings.

Keywords: Ag, Nanoprism, Nanodisk, Nanoframe, Dithiol.

RESEARCH ARTICLE

1. INTRODUCTION

Materials with hollow nanostructures potentially have low densities and large specific areas and surface permeability which are sensitive to particle sizes and could thus prove useful for various applications such as lithium-ion batteries (LIBs),[1] catalysis and sensing,[2,3] and biomedical applications.[4–7] For example Xie et al. used VOOH hollow dandelions with excellent reversible lithium storage properties to improve the lithium storage properties of VOOH solid microparticles.[1] Li et al. demonstrated the use of PdCo bimetallic hollow nanospheres catalysis to produce a high yield Sonogashira reaction[2] Zhao et al. reported that noble metal catalysts supported on hollow structures led to better electrocatalytic performance in the detection of formic acid.[3] Sokolova et al. reported the creation of DNA-loaded multishell calcium phosphate nanoparticles. The transfection efficiency using those hollow particles was significantly higher than that resulting from simply coating DNA on the surface of calcium phosphate nanoparticles.[6]

Several physical and chemical approaches involving the Kirkendall effect,[8] Ostwald ripening,[9] and galvanic replacement reaction[10] have been used to fabricate metal and metal oxide nano-hollows. Starting with Ag nano- or micro-templates, the transformation from Ag composition into Au or Au/Ag alloy hollows has been intensively studied using the galvanic replacement strategy.[10] However, few studies have reported on the fabrication of hollow Ag nanostructures.[11] The templating strategy is commonly used; for example, sacrificing templates using block polymers[12] and silica[13] to yield Ag nanoshells. For the Ag-related two-dimensional (2D) nanoframes, the vast majority of compositions were all generated in the form of Au/Ag alloy using galvanic replacement from solid Ag nanomaterials.[14] Electron beams have proven useful for to inducing morphology transformations. Latham et al. exposed amorphous metal oxide nanoparticles subjected to TEM electron beam irradiation resulting in a morphology change from solid to hollow nanoshells.[16] In addition, electron beams have been shown to cause distinct Au nanoparticles to sinter and coalescence into larger aggregates.[17] The present study adopts a different approach for fabricating hollow structures, finding that the preparation of Ag nanoframes from 2D solid Ag nanoplates is facilitated by the ripening of dithiol molecules, such as meso-2, 3-dimercaptosuccinic acid (DMSA), followed by electron beam etching. Such an approach was successfully applied to the forms of triangular prism and spherical disc.

*Author to whom correspondence should be addressed.

1533-4880/2012/12/2548/009 doi:10.1166/jnn.2012.5691

2. EXPERIMENTAL DETAILS

2.1. Materials

Trisodium citrate dihydrate (SHOWA), Poly(sodium styrenesulphonate) (PSS, Aldrich), sodium borohydride ($NaBH_4$, Lancaster), Silver nitrate ($AgNO_3$, Hwang Long), and Ascorbic acid (Riedel-de Haen) were purchased and used without further purification.

2.2. Preparation of Ag Nanoprisms and Ag Nanodisks

Ag nanoprisms were prepared using the seed-mediated method described by Aheren et al.[8] Silver seeds were produced by mixing 2.5 mM of aqueous trisodium citrate (5 mL), 0.25 mL of aqueous poly (sodium styrenesulphonate) (PSSS, MW = 25000, 500 mg L^{-1}) and 0.3 mL of aqueous $NaBH_4$ (10 mM). Subsequently, 5 mL of aqueous $AgNO_3$ (0.5 mM) were added into mixture solutions at a rate of 2 mL min^{-1} under continuous stirring. The Ag nanoprisms were prepared through the following steps: 3 mL of aqueous $AgNO_3$ (0.5 mM) were added at a rate of 1 mL min^{-1} into a mixture containing 30 μL of as-synthesized Ag seeds, 75 μL of aqueous ascorbic acid (10 mM), and 5 mL of distilled water. After 10 min of reaction in formation of Ag nanoprisms, another 0.5 mL of aqueous trisodium citrate (25 mM) was added to stabilize the nanoprisms.

In the synthesis of Ag nanodisks, 1 μL of HCl (4 M) solution was added to 5 mL of as-synthesized Ag nanoprisms, and the solution was then incubated for 10 min. The resulting colloidal solution was centrifuged at 10000 rpm for 10 min to remove the supernatants. The precipitates (Ag nanodisks) were washed with distilled water and redispersed in distilled water.

2.3. Preparation of Ag Nanoframes

The as-prepared Ag nanoprisms were mixed with DMSA at various DMSA concentrations (0.01, 0.05, 0.1, and 0.5 mM) under stirring for 4 h in the dark. The resulting colloids were then subjected to further characterization including TEM, XRD, and XPS measurements. Notably, in addition to providing morphology observation and structural characterization, TEM provided the electron beam etching process to form nanoframe structures. Ag nanorings were prepared following the same approach using electron beams.

2.4. Characterization

Electron micrographs were obtained using transmission electron microscopes (JEOL 3010 at 80 keV and PHILIPS CM-200 at 200 keV). X-ray diffraction (XRD) results were collected on a diffractometer (Rigaku D-Max IIIV) using Cu Kα radiation ($\lambda = 1.54056$ Å) at 30 kV and 30 mA. IR spectra were measured using a KBr plate in a Fourier transformation infrared (FTIR) spectrometer (200 E; Jasco International Co., Ltd., Tokyo, Japan). X-ray photoelectron spectra (XPS) (VG Scientific 210) were recorded using an Mg Kα source(12 keV and 10 mA). The binding energy scale was calibrated to 284.6 eV for the main (C ls) peak.

3. RESULTS AND DISCUSSION

Taking triangular plates as an example, Scheme 1 presents the typical ripening and etching/sintering processes in the solid 2D Ag nanoprisms. Dithiol molecules with two–SH groups are expected to play the crucial role of fixing the detached particles. A seed-mediated method was used to prepare Ag nanoprisms.[18] The as-prepared Ag nanoprisms displayed mostly as truncated triangular structures with an edge-length of ~78 nm and a thickness of ~6.9 nm (TEM image in Supporting Information Fig. 1(a)). The corresponding UV-vis spectrum (Fig. 1(b)) exhibited two apparent plasmon resonance features at 798 nm (in-plane dipole) and 332 nm (out-of-plane quadrupole).[18] A shoulder located between 500 and 600 nm is attributed to in-plane quadrupole resonance. The resulting Ag nanoprisms were then incubated with DMSA for 4 h, and subsequently exposed to electron beam irradiation using a transmission electron microscope (TEM). The DMSA was dissolved in ethanol and mixed with aqueous Ag colloids. Figure 2 shows the morphology of Ag nanoframes in the course of continuous exposure to the electron beam. Electron beam irradiation transformed the Ag solid nanoprisms into nanoframes. This electron-induced structural change occurred rapidly, and the transformation was carefully and repeatedly documented. Initially, many small particles seemed to be ripped off from the surface of the nanoprisms and aggregated along the prism edges in the form of triangular shells with a thickness of ~12 nm (Fig. 2(a)).

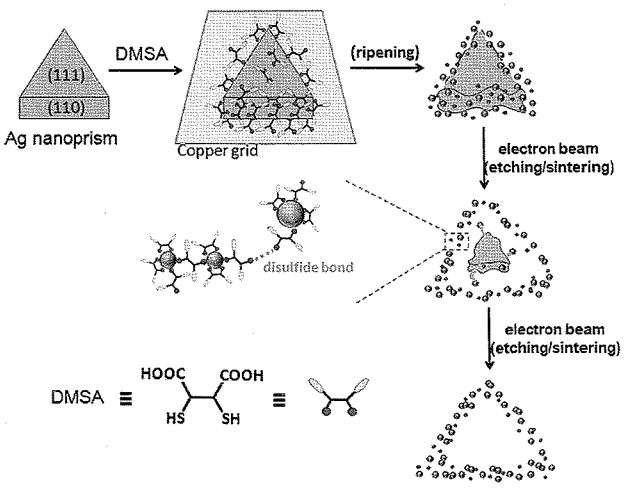

Scheme 1. Ag triangular nanoframe formation process following DMSA ripening and electron beam etching.

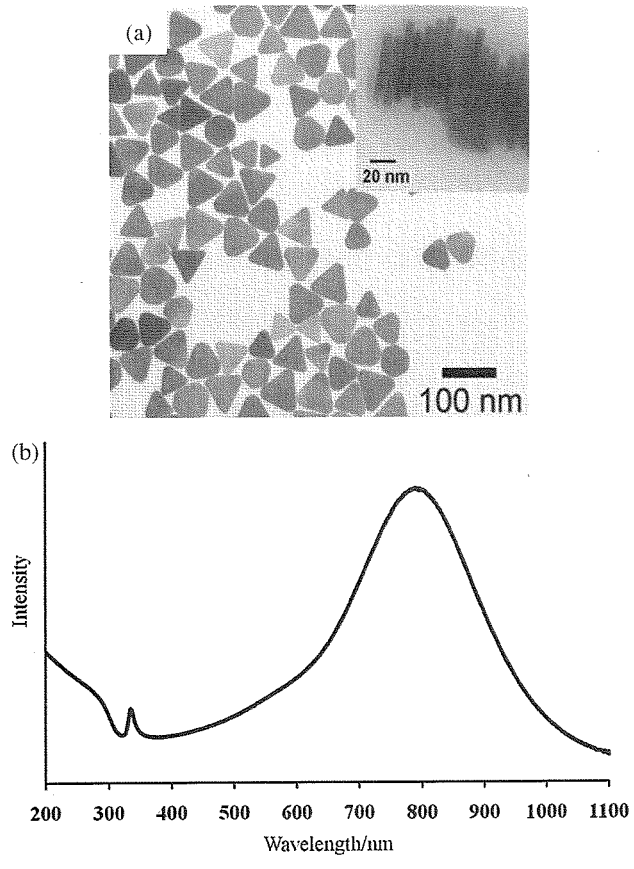

Fig. 1. (a) TEM image of Ag nanoprisms. Inset shows close-packed nanoprisms in a vertical orientation. (b) UV-Vis extinction spectrum of Ag nanoprisms dispersed in water.

Upon electron beam radiation, some nanoprisms quickly formed a void between the core and shell to become core/void/shell structures. Continuous irradiation resulted in the inner cores shrinking and eventually evolving into nanoframe structures. It should be noted that the electron beam also induced the calescence and sintering of detached small nanoparticles. The arrows indicate a representative nanoprism showing the evolutionary process (Fig. (2)). The final triangular nanoframes have a slightly increased size with an edge of ~83 nm and a shell of ~15 nm. Prolonging the incubation period between Ag nanoframes and DMSA, e.g., for a week, resulted in the same structural transformation upon electron exposure. In the absence of electron beam irradiation (i.e., purely incubating Ag prisms with DMSA) did not induce any hollowing. Notably, the morphology of Ag nanoprisms without DMSA treatment was not affected by the electron beam exposure.

Through the observation of ripening and etching processes to form Ag nanoframes, we studied the effect of DMSA concentration. Figure 3 shows TEM images for Ag nanoframes incubated in a series concentrations (0.01, 0.05, 0.1, and 0.5 mM) of DMSA. All of the images were taken at exposures of 1 min. At a low concentration of 0.01 mM (Fig. 3(a)), a lower degree of ripening was observed accompanied with the detachment of a few nanoparticles from the nanoprisms. Extending electron beam radiation produced no additional etching. However, Ag nanoframes were generated when the DMSA concentration was increased to 0.05 mM, seemingly implying that a certain degree of DMSA concentration is required to effectively ripen nanoprisms and allow electron beam corrosion. If we closely examined the resulting sphere-like nano-domains in the nanoframes, concentrations of 0.01 and 0.05 mM led to larger particle domains in the range of 3–5 nm (Figs. 3(a and b)), while the 0.1 and 0.5 mM concentrations yielded sizes of <3 nm (Figs. 3(c and d)). Higher concentrations with more DMSA molecules resulted in smaller particles being ripped off. It is known that small particles have a lower melting temperature and a higher sintering rate than larger particles.[17] Thus, in the course of electron beam irradiation, the sintering of nanoparticles was readily observed at higher DMSA concentrations. Note that the sphere-like particle (indicated by the arrow) seen in Figure 3(c) originated from the as-prepared Ag prism samples. In our preparation of Ag nanoprisms, the spherical particles appeared in a distribution of <10%.

The DMSA treated-Ag nanoprisms were collected from the colloidal solutions for XRD, FT-IR, XPS, and Raman measurements. The relevant DMSA treated-Ag nanoprism samples were characterized without electron beam exposure. X-ray diffraction (XRD) measurements were conducted to characterize Ag nanoprisms before and after treatment with DMSA (0.05 mM) (Fig. 4). The DMSA-treated Ag nanoprisms exhibited the exact same patterns as Ag nanoprisms and retained an Ag structure. FT-IR analysis (Fig. 5) was performed to identify the co-existence of DMSA adsorption and citrate ions on Ag nanoprisms with the presence of ~1585 cm^{-1} and ~1395 cm^{-1} of the COO^- vibrations from sodium citrate and ~1703 cm^{-1} of the C=O vibration of DMSA. Our preparation used sodium citrates to synthesize the Ag seeds and to stabilize the Ag nanoprisms. It has been reported that the crystallographic planes of Ag nanoprisms include (111) basal planes and (110) side planes[19] and prefer to cap more citrate ions on the (111) planes.[20] X-ray photoelectron spectroscopy (XPS) was conducted to measure the core-level binding energies of Ag3d and S2p for 0.05 mM of the DMSA-treated Ag nanoprisms. Two sharp splitting peaks at 368.4 and 374.4 eV respectively correspond to Ag $3d_{3/2}$ and $3d_{5/2}$ (Fig. 6(a)). The peaks shift 0.4 eV to a higher binding energy relative to bulk Ag.[21] However, a broad band was observed for S2p. The deconvolution of the peak with respect to Gaussian fitting resolved three peaks: two at 162.1, 163.3, corresponding respectively to $S2p_{3/2}$ and $S2p_{1/2}$, and one at 163.7, assigned to the disulfide bond. The S2p doublet peaks of the DMSA-treated Ag nanoprisms appear at lower binding energies.

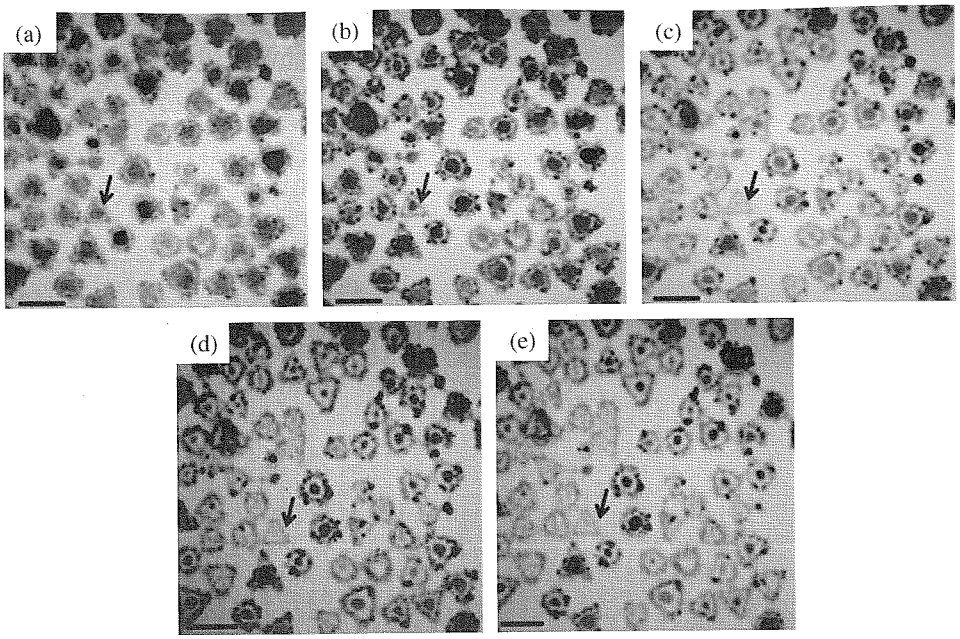

Fig. 2. Sequential TEM images of Ag nanoprisms incubated with DMSA (0.05 mM) for 4 h, then subjected to electron beam (80 keV, 15 μA, current density: 5.24×10^{-12} C/cm^2) irradiation as a function of exposure time: (a) 0 s; just after electron beam irradiation started, (b) 6 s (c) 10 s, (d) 12 s, and (e) 16 s. All scale bars are 100 nm.

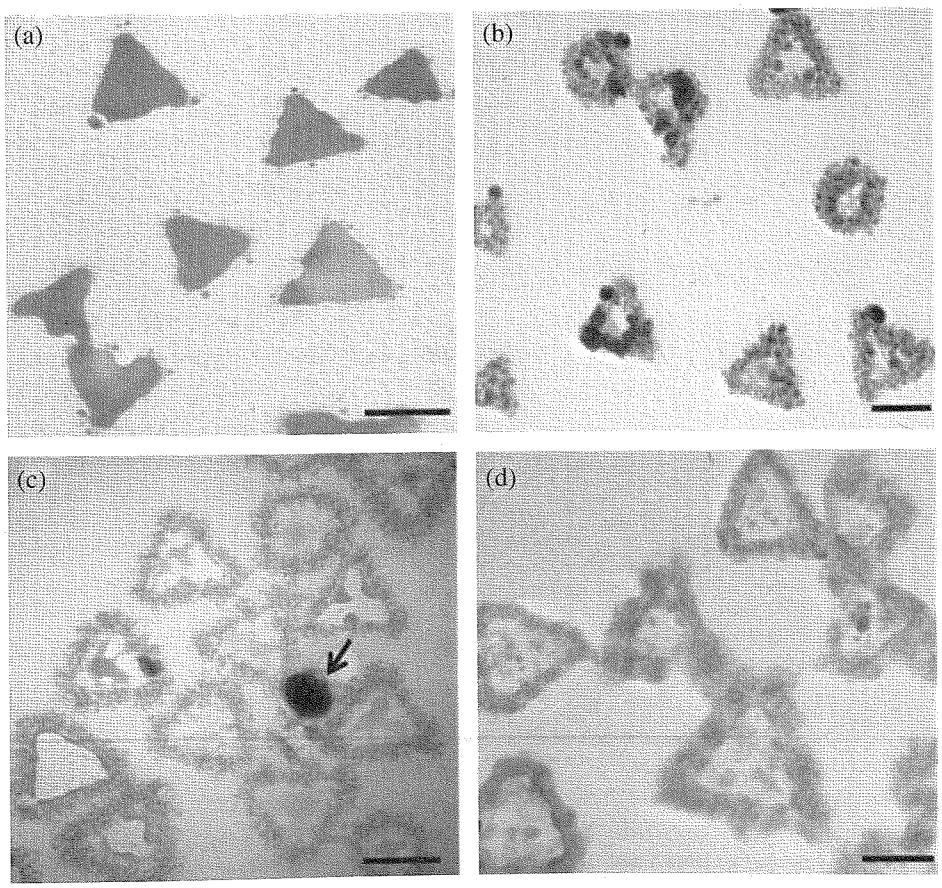

Fig. 3. TEM images of Ag nanoprisms incubated with DMSA concentrations of (a) 0.01 mM, (b) 0.05 mM, (c) 0.1 mM, and (d) 0.5 mM for 4 h, and then subjected to electron beam irradiation (200 keV, 100 μA, current density: 40.8 pA/cm^2) for 1 min. All scale bars are 50 nm.

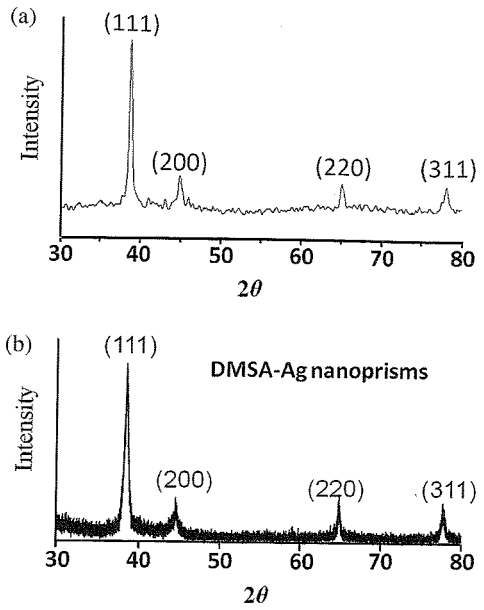

Fig. 4. X-ray diffraction patterns of (a) Ag nanoprisms and (b) DMSA-treated Ag nanoprisms. For DMSA-treated Ag nanoprisms, Ag nanoprisms were incubated with 0.05 mM of DMSA for 4 h, and then collected for XRD measurements.

The chemical shifts to a higher binding energy for Ag3d and to a lower binding energy for S2p indicate DMSA was adsorbed on the Ag nanoprisms in a form of Ag^{+}–S^{-}. Raman characterization provides further evidence of a disulfide group (Fig. 6(b)). Figure 6(c) shows the elemental analysis of a single Ag nanoframe. Very little Ag or S was detected in the center region of the nanoframe. The small Ag and S signals are likely due to the beam spot coverage on some frame edges. Meanwhile, the apparent Ag and S signals appeared when analyzing the border frame. No electron diffraction pattern was observed when the center region was captured. Together, these analyses indicate that the Ag nanoframe structure has a void core and a two-dimensional frame. HRTEM analysis indicates the Ag nanoframes having a mixed crystallinity with small nanoparticles having a single crystalline structure with lattice fringes of 2.4 Å corresponding to the {111} planes while some domains showed no crystalline structure (Fig. 7).

To gain insight into the formation of nanoframes, we investigated mercaptosuccinic acid which has a similar organosulfur structure. It was found that mercaptosuccinic acid has a weak ripening ability. Figure 8(a) shows some nanoparticles detached from nanoprisms through 2 min of electron beam exposure in the absence of nanoframe formation. An inverse Ostwald ripening to form monodisperse nanoparticles, known as digestive ripening, exhibits a process of disintegrating large particles in favor of small particles.[22] It has been suggested that the ability to break large particles into smaller particles is associated with the interaction of a metal surface (Au, Ag) with ripening agents.[23] Thus, it may follow that the binding to Ag nanoprisms is stronger for DMSA than for mercaptosuccinic acid. Since the DMSA structure can be seen as being composed of two 2-mercaptoacetic acid skeletons, we next examined the 2-mercaptoacetic acid effect. As seen in Figure 8(b), many small particles have broken away from the Ag nanoprisms. The 2-mercaptoacetic acid exhibited a strong ripening effect and the disintegration process can be observed down to 0.005 mM. We captured a single Ag nanoprism to monitor its structural evolution as a function

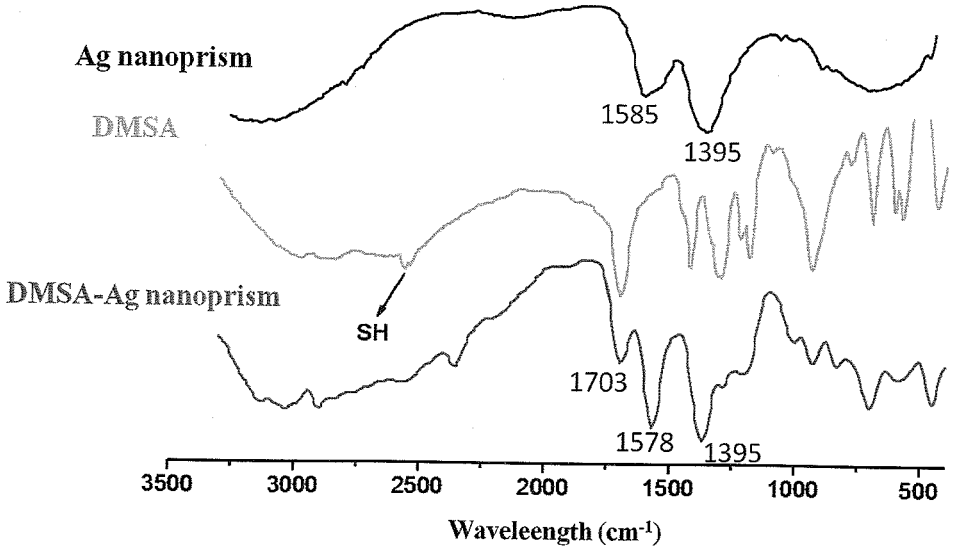

Fig. 5. FT-IR spectra of Ag nanoprisms, free DMSA and DMSA-treated Ag nanoprisms. For DMSA-treated Ag nanoprisms, Ag nanoprisms were incubated with 0.05 mM of DMSA for 4 h, and then collected for FT-IR measurements. The ~1585 cm^{-1} and ~1395 cm^{-1} of the Ag nanoprisms corresponds with the COO^{-} vibrations of sodium citrate. The ~1703 cm^{-1} of free DMSA is associated with the C=O vibration from DMSA. The DMSA treated-Ag nanoprisms appeared at ~1578 cm^{-1} and ~1395 cm^{-1} of asymmetric and symmetric COO^{-} vibrations from sodium citrate with ~1703 cm^{-1} contributed from C=O vibration of DMSA.

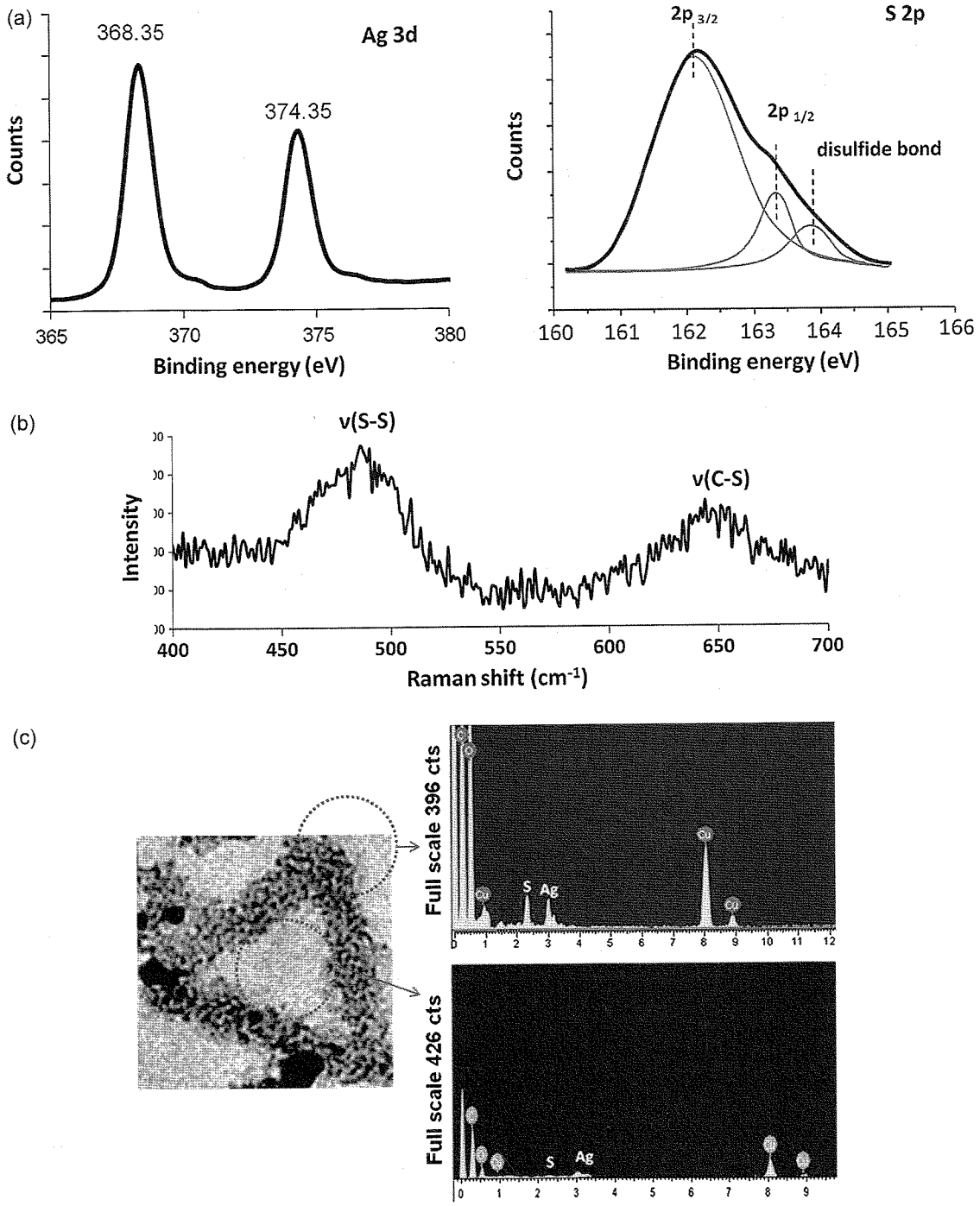

Fig. 6. (a) XPS spectra of DMSA-treated Ag nanoprisms revealing core levels of Ag3d and S2p. (b) Raman characterization of DMSA-treated Ag nanoprisms. (c) High-resolution TEM image (current density: 40.8 pA/cm^2) and the corresponding EDX analysis of Ag nanoframes. The red circled region focus on the middle part of nanoframes, while the blue circled region inspected the frame. For DMSA-treated Ag nanoprisms, Ag nanoprisms were incubated with 0.05 mM of DMSA for 4 h, and then collected for measurements.

of beam irradiation time. Figure 8(c) shows the collapse of 2-mercaptoacetic acid treated Ag nanoprisms. We have speculated that, unlike 2-mercaptoacetic acid with only a single thiol group, the two S-H groups of dithiol DMSA, could bind directly to two neighboring particles in addition to concerning ripening process. Additionally, the formation of disulfide bonds should provide an extra linkage to which to attach different particles to yield a triangular frame (Scheme 1).

Taken together, these results suggest that the fabrication of nanoframes involves ripening behavior through the use of dithiols, followed by electron beam corrosion. The

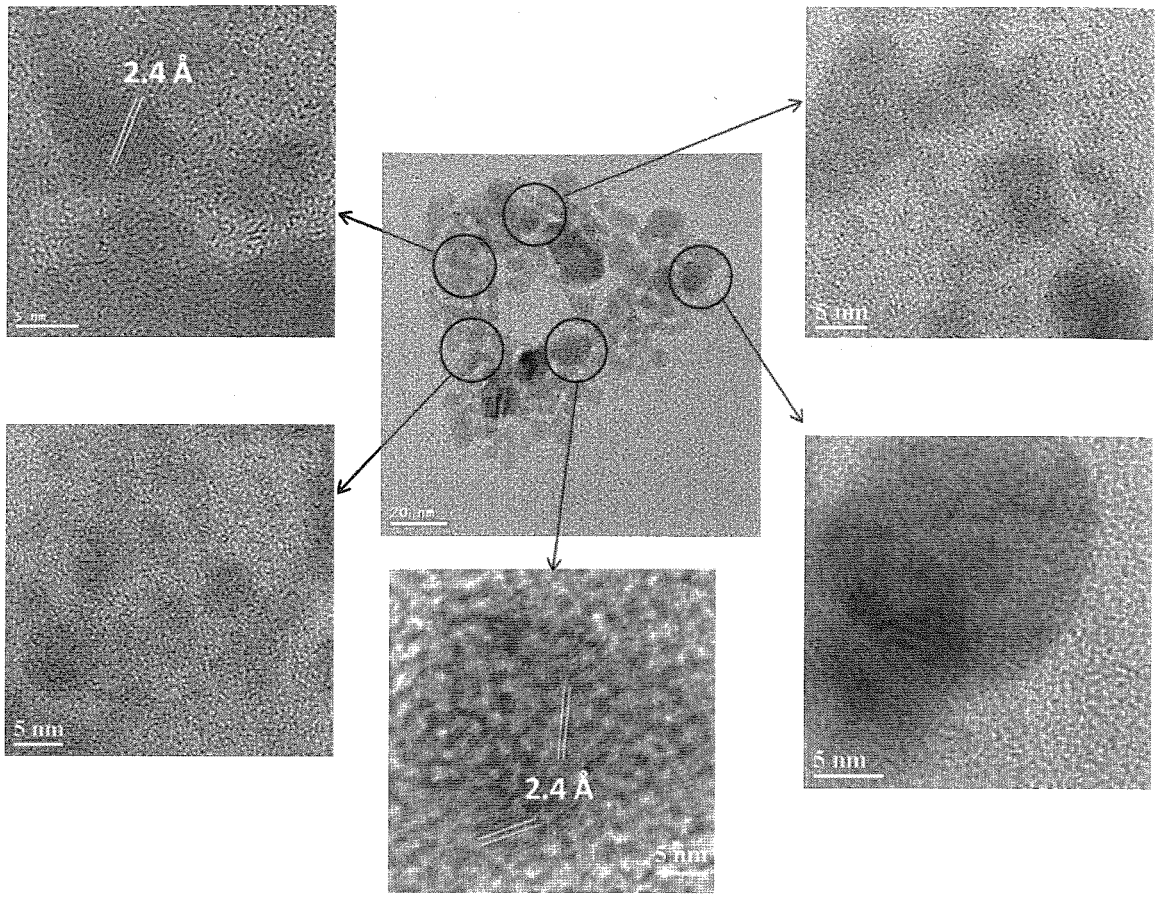

Fig. 7. High-resolution TEM images of Ag nanoframes. The circled regions indicate the corresponding particle domains. The Ag nanoprisms were incubated with 0.05 mM of DMSA for 4 h (current density: 40.8 pA/cm^2).

presence of two –SH groups and the formation of disulfide bonds facilitates the linking of nano-domains resulting in the triangular shape. The structural transformation from solid prism to hollow frame is complex. It is possible that the ripening to break large particle into smaller ones could create significant defects and voids on the Ag nanoprism surface. Such defects are energetically-favorable paths for metal diffusion outward to the surface.[8, 24] The vacancies migrate along these defects and begin to coalesce and merge with the initial voids created by ripening. Over time, electron beam irradiation causes the voids to continuously grow until the interior of the Ag core is consumed. Based on the XPS results, the interaction of DMSA with the Ag nanoprisms resembles an Ag^+–S^- form. It is possible that the electron beam reduction process yields Ag atoms accompanying the outward diffusion. The resulting Ag atoms coalescence into clusters, and then grow into nanosized particles.[25] It is known that the (110) side planes in Ag nanoprisms have a greater surface energy than the (111) basal planes[19] and the {111} planes are passivated by more citrate ions. We believe that the dithiols can be expected to favorably attach on the {110} side planes resulting in significant ripening which produces many small particles along the edge. In addition, we cannot exclude the possibility that the localized heat was generated by electron beam irradiation. The additional heating factor provided in the microscope can contribute to particle morphology changes. The electron beam produced local heating to cause atomic motion and rearrangement. The hollowing process was derived by the outward diffusion of metal atoms in the nanoparticles enabled by the high local temperature upon exposure to the electron beam.[26]

Subsequently, we extended the nano-architecture to the 2D nanodisc using DMSA. In the synthesis of Ag nanodiscs, 1 μL HCl (4 M) was added into 5 mL of Ag nanoprism colloidal solution, and then incubated for 10 min. The resulting Ag nanodiscs had an average size of ~50 nm and an increased thickness of ~10 nm (Fig. 9(a)). The UV-vis spectrum (Fig. 9(b)) of the Ag nanodiscs exhibited plasmon resonance features at 508 nm (in-plane dipole) and 337 nm (out-of-plane quadrupole).[27–30] Following the same procedure as that for nanoprisms, nanodiscs were incubated with DMSA for 4 h. Interestingly, nanodiscs seem to be more energetically stable than nanoprisms, in which the significant ripening behavior occurred until the concentration of DMSA was raised to 5 mM. Figure 9(c) shows the resulting nanorings following a DMSA ripening-electron beam etching process. The shell thickness of the nanorings ranges from 8~12 nm.

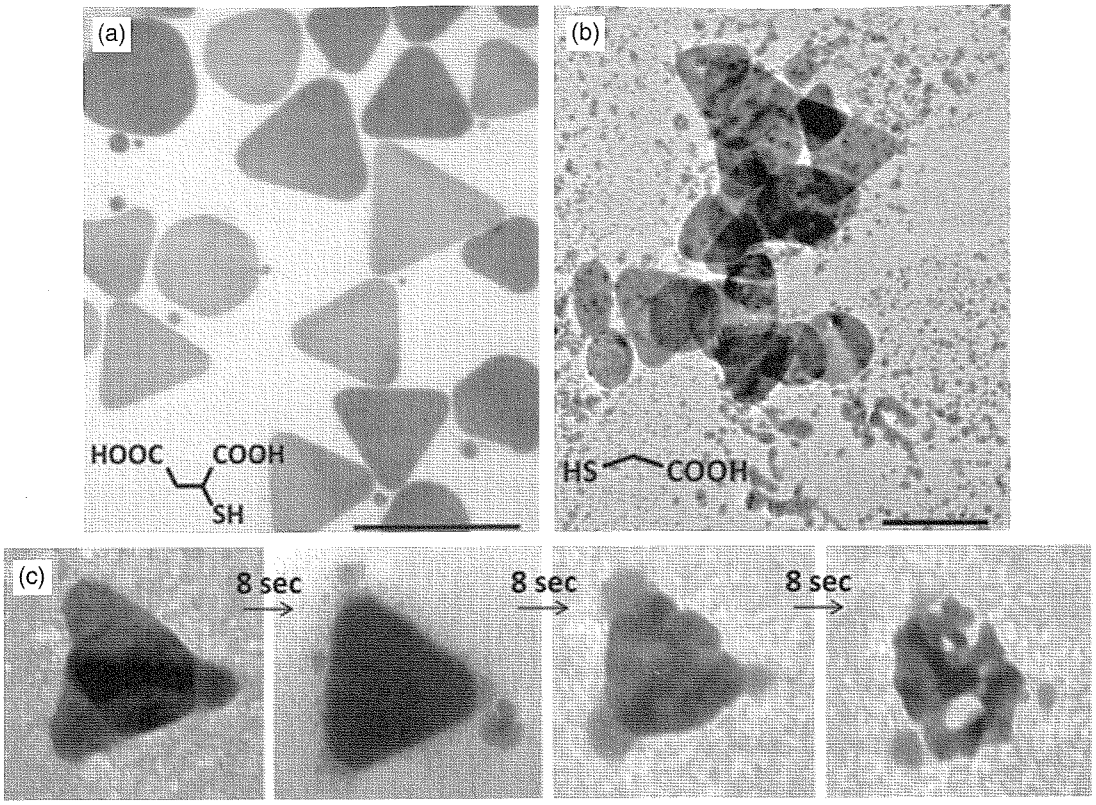

Fig. 8. TEM images of Ag nanoprisms incubated with 0.05 mM of (a) mercaptosuccinic acid and (b) 2-mercaptoacetic acid, followed by 2 min electron beam exposure, (c) sequential TEM images of Ag nanoprisms incubated with 0.05 mM of 2-mercaptoacetic acid for 4 h, then exposed to the electron beam as a function of exposure time. The displayed TEM images were all exposed to 80 keV electron beam with 15 μA (current density: 5.24×10^{-12} C/cm^2). The scale bars are all 100 nm.

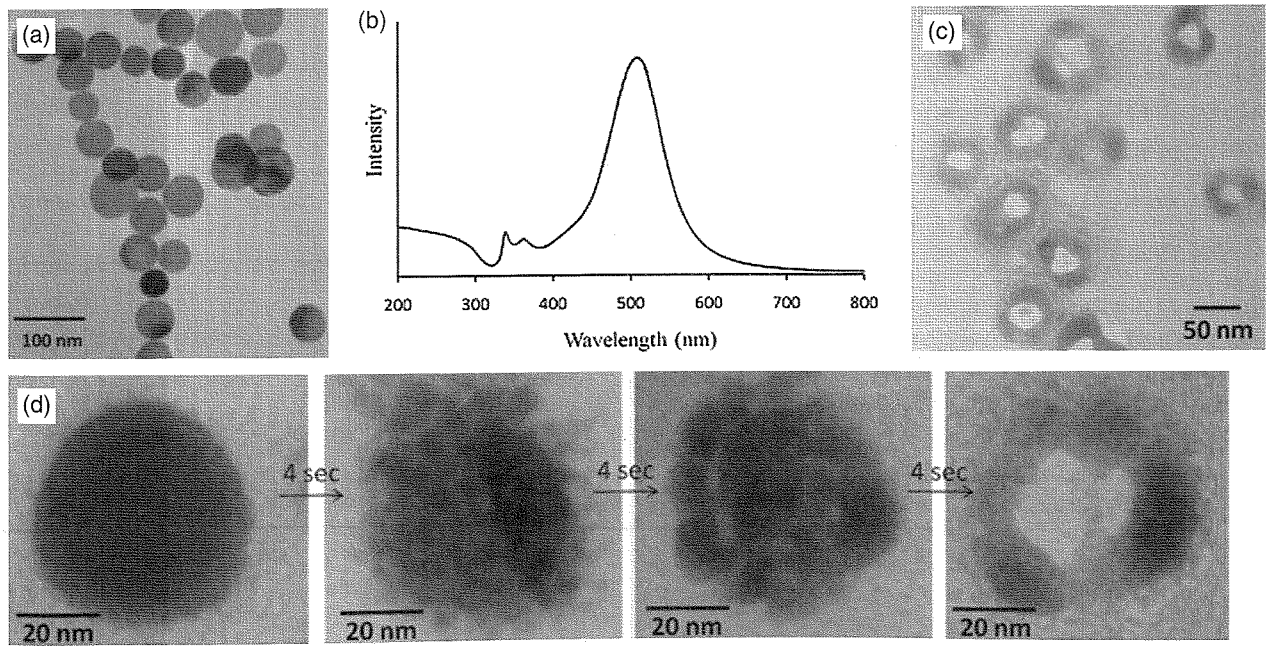

Fig. 9. (a) TEM image of Ag nanodiscs. (b) UV-vis spectrum of Ag nanodiscs. (c) TEM images of Ag nanorings. (d) Sequential TEM images of Ag nanodiscs incubated with 5 mM of DMSA for 4 h, then exposed to the electron beam as a function of exposure time. The displayed TEM images were all exposed to 80 keV electron beam with 15 μA (current density: 5.24×10^{-12} C/cm^2).

The TEM images shown in Figure 9(d), monitored upon electron beam irradiation, reveal a structural evolution leading to nanoring structure, where the nanodiscs underwant ripening and beam etching in conjunction with the sintering process.

4. CONCLUSIONS

Assisted by dithiols and electron beam radiation, 2D nanoarchitectures treated with DMSA showed a transformation of solid Ag nanoprisms and nanodiscs into hollow nanoframes and nanorings. X-ray photoelectron spectroscopy (XPS) determined the surface chemical compositions and indicated DMSA adsorbed on the Ag nanoprisms in the form of Ag^{+}–S^{-}. It is possible that the electron beam reduction process yielded Ag atoms accompanying outward diffusion of the metal atoms. Over time, electron beam irradiation caused the voids to grow until the interior of the Ag core was consumed. Localized heat from the electron beam irradiation possibly contributed to atomic motion and rearrangement and enabled a hollowing process derived by the outward diffusion of metal atoms. Studies of the similar organosulfur structures such as mercaptosuccinic acid and 2-mercaptoacetic acid suggested that the two S-H groups of dithiol DMSA played the crucial role in the fabrication of nanoframes. Interesting, we have found that the Ag nanodiscs are more resistant to DMSA ripening in Ag nanodiscs than in nanoprisms because of the higher DMSA concentration required to form nanorings It is anticipated that the approach used in this study can be further developed for the patterning of 2D Ag nanofilms.

Acknowledgments: This work was supported by the National Science Council of Taiwan.

References and Notes

1. J. M. Tarascon and M. Armand, *Nature* 414, 359 (**2001**).
2. Y. G. Li, P. Zhou, Z. H. Dai, Z. X. Hu, P. P. Sun, and J. C. Bao, *New J. Chem.* 30, 832 (**2006**).
3. J. Zhao, W. X. Chen, Y. F. Zheng, and X. Li, *J. Power Sources* 162, 168 (**2006**).
4. J. Zhou, W. Wu, D. Caruntu, M. H. Yu, A. Martin, J. F. Chen, C. J. O'Connor, and W. L. Zhou, *J. Phys. Chem. C* 111, 17473 (**2007**).
5. C. Loo, A. Lowery, N. Halas, J. West, and R. Drezek, *Nano Lett.* 5, 709 (**2005**).
6. V. V. Sokolova, I. Radtke, R. Heumann, and M. Epple, *Biomaterials* 27, 3147 (**2006**).
7. K. An and T. Hyeon, *Nanotoday* 4, 359 (**2009**).
8. Y. Yin, R. Rioux, C. K. Erdonmez, S. Hughes, G. A. Somorjai, and A. P. Alivisatos, *Science* 304, 711 (**2004**).
9. H. G. Yang and H. C. Zeng, *J. Phys. Chem. B* 108, 3492 (**2004**).
10. L. Au, X. Lu, and Y. Xia, *Y. Adv. Mater.* 20, 2517 (**2008**).
11. C. L. Lee, C. M. Tseng, R. B. Wu, and K. L. Yang, *Nanotechnology* 19, 215709 (**2008**).
12. K. T. Yong, Y. Sahoo, M. T. Swihart, and P. N. Prasad, Colloids and Surfaces A, *Physicochem. Eng. Aspects.* 290, 89 (**2006**).
13. Z. Wang, X. Chen, M. Chen, and L. Wu, *Langmuir* 25, 7646 (**2009**).
14. L. Au, X. Lu, and Y. Xia, *Adv. Mater.* 20, 2517 (**2008**).
15. X. Lu, H. Y. Tuan, J. Chen, Y. Z. Li, B. A. Korgel, and Y. Xia, *J. Am. Chem. Soc.* 129, 1733 (**2007**).
16. A. H. Latham and M. E. Williams, *Langmuir* 24, 14195 (**2008**).
17. Y. Chen, R. E. Palmer, and J. P. Wilcoxon, *Langmuir* 22, 2851 (**2006**).
18. A. Damian, M. L. Deirdre, G. Matthew, and M. K. John, *Adv. Funct. Mater.* 18, 2005 (**2008**).
19. R. Jin, Y. W. Cao, C. A. Mirkin, K. L. Kelly, G. C. Schatz, and J. G. Zheng, *Science* 294, 1901 (**2001**).
20. Y. Sun and Y. Xia, *Adv. Mater.* 15, 695 (**2003**).
21. L. Cheng, X. Liu, J. Lei, and H. Ju, *Anal. Chem.* 82, 3359 (**2010**).
22. K. V. G. K. Murty, M. Venkataramanan, and T. Pradeep, *Langmuir* 14, 5446 (**1998**).
23. S. Y. Kang and K. Kim, *Langmuir* 14, 226 (**1998**).
24. J. Jnschek, U. Kaiser, and W. Richter, *Japanese Society of Electron Microscopy.* 50, 3 (**2001**).
25. J. U. Kim, S. H. Cha, K. Shin, J. Y. Jho, J. C. Lee, and J. Am, *Chem. Soc.* 127, 9962 (**2005**).
26. A. H. Latham and M. E. Williams, *Langmuir* 24, 14195 (**2008**).
27. J. An, B. Tang, X. Zheng, J. Zhou, F. Dong, S. Xu, Y. Wang, B. Zhao, and W. Xu, *J. Phys. Chem. C* 112, 15176 (**2008**).
28. X. Zou, E. Ying, H. Chen, and S. Dong, Colloids and Surfaces A *Physicochem. Eng. Aspects.* 303, 226 (**2007**).
29. X. Jiang, Q. Zeng, and A. Yu, *Nanotechnology* 17, 4929 (**2006**).
30. S. Chen, Z. Fan, and D. L. Carroll, *J. Phys. Chem. B* 106, 10777 (**2002**).

Received: 1 July 2011. Accepted: 30 August 2011.